Highly Packed and Oriented DNA Mesophases Identified Using in Situ Microfluidic X-ray Microdiffraction

Thomas Pfohl,*,† Alexander Otten,† Sarah Köster,†,‡ Rolf Dootz,† Bernd Struth,§,|| and Heather M. Evans†

Max Planck Institute for Dynamics and Self-Organization, Bunsenstrasse 10, D-37073 Göttingen, Germany, and European Synchrotron Radiation Facility, 6 Rue Jules Horowitz, BP 220, 38043 Grenoble Cedex, France

Received March 20, 2007; Revised Manuscript Received May 3, 2007

DNA condensation in vivo usually requires proteins and/or multivalent salts. Here, we explore the in vitro compaction of DNA by cationic dendrimers having an intermediate size and charge. The dynamic assembly of DNA−dendrimer mesophases is discernible due to the laminar flow in a specially designed X-ray compatible microfluidic device. The setup ensures a nonequilibrium ascent of reactant concentration, and the resulting progression of DNA compaction was detected online using microfocused small-angle X-ray diffraction. The evolution of a DNA−dendrimer columnar square mesophase as a function of increasing dendrimer content is described. Additionally, in regions of maximum shear, an unexpected high-level perpendicular ordering of this phase is recorded. Furthermore, these assemblies are found to be in coexistence with a densely packed DNA-only mesophase in regions of excess DNA. The latter is reminiscent of dense packing found in bacteriophage and chromosomes, although surprisingly, it is not stabilized by direct dendrimer contact.

Introduction

The in vivo compaction of DNA demonstrates nature's sophisticated strategies for packing, protection, and exchange of genetic information.[1−3] Reversible packing mechanisms enable essential cellular tasks such as replication and transcription. The consecutive hierarchical organization of chromatin and the formation of DNA assemblies with the DNA-binding protein Dps in bacteria under nutritional stress are two prominent real-life examples of compaction processes.[2,3] From a more fundamental point of view, DNA compaction is characterized by challenging problems of phase transitions, liquid crystal behavior, and polyelectrolyte interactions.[4−6]

In the present work, cationic dendrimers were used to compact DNA. These molecules act as a model system to mimic the influence of electrostatic interactions on in vivo DNA compaction. The fourth generation dendrimers (G4) used here have a size ($R = \sim$1.6 nm) and charge (62^+) that is conveniently between that of small multivalent salts and larger proteins such as histones.[7] Recently, DNA−dendrimer assemblies have been explored as possible non-viral gene vectors in therapeutic applications.[8−11] The resulting interest in dendrimers stemming from both biology and physics has motivated many studies of these molecules either alone or when complexed with DNA.[7,8,10−13] The majority of the latter utilizes techniques such as optical density measurements, circular dichroism, and neutron scattering.[7,13,14]

Small-angle X-ray diffraction is a particularly useful tool for studies of DNA compaction since it probes relevant length scales (on the order of nanometers) and can illuminate multidimensional details of DNA mesophases—particularly when assemblies are aligned.[15,16] Evans et al. previously reported a rich phase diagram of stable G4−DNA complexes, identified using diffraction.[17] Similar techniques were used to identify a comparable assembly of DNA and starburst (PAMAM) dendrimers.[18] However, the use of synchrotron radiation can damage the sample, and typically, bulk samples are prepared in advance and require large amounts of raw material. Perhaps most importantly, bulk experiments are not amenable to online variations of DNA condensation conditions and measurements as are those we report here.

We describe a microfluidic experiment probing the real-time dynamic evolution of the supramolecular interactions between DNA and cationic dendrimers. Microfluidic techniques are particularly useful for investigations of biomaterials. The miniaturization, integration, and analysis of chemical and biological processes on the nanoliter scale continues to drive remarkable progress in the fields of biotechnology, protein crystallization, and combinatorial chemistry.[19−23] Aside from advantages such as reduced sample volumes and the possibility of high throughput and parallel operations, microfluidics is a powerful tool for fundamental investigations of soft condensed matter and biological systems.[24] The interesting physics of fluid flow on the micro- and nanoscale enables controlled manipulation of even single macromolecules.[25]

Two-dimensional columnar mesophases of G4−DNA were identified for different charge ratios using microfocused X-ray diffraction. In addition, we found a previously unobserved mesophase oriented transverse to the flow direction in regions of maximum shear. Using the microflow device, we were also able to pinpoint reaction dynamics at low charge ratios below the isoelectric point, where DNA is in excess. In this regime, we discovered a densely packed DNA-enriched mesophase. This result implies an alternate route of DNA compaction aside from established salt or macroion condensation.[26−28]

* Corresponding author. E-mail: thomas.pfohl@ds.mpg.de.
† Max Planck Institute for Dynamics and Self-Organization.
‡ Present address: Department of Physics, Harvard University, 40 Oxford St. ESL 201, Cambridge, MA 02138.
§ European Synchrotron Radiation Facility.
|| Present address: HASYLAB at DESY, Notkestrasse 85, D-22603 Hamburg, Germany.

10.1021/bm070317s CCC: $37.00
Published on Web 06/19/2007

Experimental Procedures

Materials. Polypropyleneimine dendrimers generation 4, G4, (DAB-Am-32, Sigma-Aldrich Chemie GmbH, Taufkirchen, Germany) were solubilized in ultrapure 18.2 MΩ cm water (Millipore GmbH, Schwalbach, Germany) to a final concentration of 20 mg/mL. DNA solutions were similarly prepared at 10 mg/mL using lyophilized highly polymerized calf thymus DNA (Sigma-Aldrich Chemie GmbH, Taufkirchen, Germany).

Microflow Devices. The microchannels (width of 150 μm) were spark eroded into 300 μm thick stainless steel plates and covered with thin adhesive Kapton foils (Dr. Müller, GmbH, Ahlhorn, Germany). The channels were connected to custom-made microsyringe pumps via Teflon tubing (Novodirect GmbH, Kehl, Germany). The flow velocities were on the order of 100 μm/s. Specific v_{DNA} and v_{G4} are given in the figure captions.

Microfocused Small-Angle X-ray Measurements. Two-dimensional scattering patterns were collected using a CCD detector with a fluorescent screen at Beamline ID10b at the European Synchrotron Radiation Facility in Grenoble, France. Beryllium compound refractive lenses (CRL)[29] focused the X-ray beam of 8 keV ($\lambda = 1.55$ Å) down to a diameter of 20 μm. The microchannel device was loaded on an $x-y$ stage, to probe specific positions using the microfocused X-ray beam. The positional accuracy of absolute coordinates in the microdevice (i.e., $x, y = 0$) was on the order of the beam size. CCD images were collected with exposure times of 30 s per position. Plots of X-ray data in the figures are offset for clarity. Baseline values of intensity for azimuthal integrations are included in the data plots.

Finite Element Modeling. FEMLab software (Comsol, Inc., Burlington, MA) was used to perform finite element modeling simulations of conditions within the microchannel device. The incompressible Navier−Stokes equation was solved in two dimensions using about 20 000 elements to obtain a solution for the diffusive mixing of dendrimers. The velocity field (and corresponding strain rate per position) and concentration profiles were subsequently calculated, using material constants (D, η) enumerated in the text. Despite the fact that the liquids were assumed purely Newtonian and that possible anisotropy due to the DNA−dendrimer assemblies have not been included, the simulations compare favorably with the flow profile seen in experiments.[30]

Results and Discussion

Microfluidic Tools Are Modified for Small-Angle X-ray Scattering Studies. The work described here takes advantage of specific flow designs to investigate the nonequilibrium dynamics of DNA compaction—at multiple reaction points—in a single microfluidic device. This is achieved by creating a well-defined gradient of chemical reactants. The flow in the devices is laminar (Reynolds number Re < 1), meaning that the mixing of components is diffusion controlled.[24] The flow velocities are chosen such that a concentration gradient of the reactants extends along the measurable length of the device. It follows that every accessible point along the reaction channel reflects a different extent of DNA compaction. In addition, the mixing of components in this well-defined manner reduces the likelihood of the creation of kinetically trapped phases. The experimental parameters employed here are such that the reaction rate of G4−DNA complexation is much faster than our observations; this statement is supported by Raman spectroscopy measurements along single stream lines in a similar setup.[30]

The hydrodynamic focusing device used here was a perpendicularly crossed microchannel having a depth of 300 μm and a width of 150 μm. A lateral scanning of the sample allows for spatially resolved small-angle X-ray diffraction experiments along the microfluidic channels (Figure 1a). An incoming flow

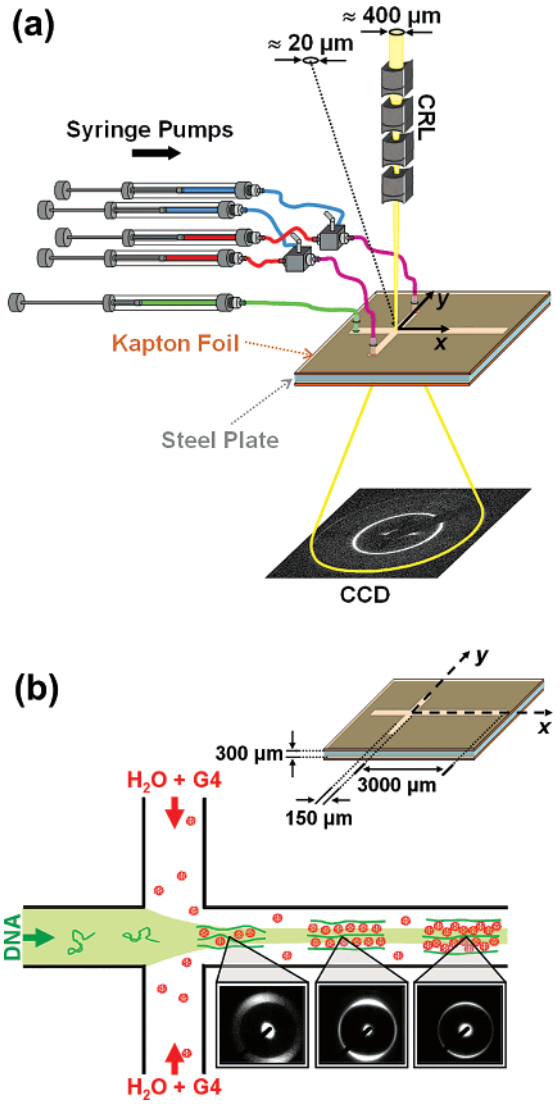

Figure 1. Experimental setup. (a) Microdevice, made from a steel plate sealed with kapton foil, was placed in a microfocused X-ray beam, and a diffraction pattern was acquired. Fluids were injected using a custom-built syringe setup. (b) Close-up schematics of the device showing relevant length scales. DNA was injected from the left and was focused by two side streams containing dendrimers (representative X-ray images also shown).

of aqueous DNA solution was hydrodynamically focused by the influx of aqueous solutions of cationic G4 dendrimers injected into the two side channels (Figure 1b). The concentration of the dendrimers in the side channels was determined by the co-flow of G4 and water into an upstream T-valve, which allowed online control of G4 concentration. The width of the focused DNA solution stream can be adjusted by the ratio of flow rates of the main channel and the side channels. Therefore, the mixing and the concentration distributions in the outlet channel can be adjusted by changing the width of the focused DNA solution stream as well as the velocities in all channels. Consequently, the interaction dynamics depending on the concentration distribution can be spatially separated in the steady-state flow.

The velocity and concentration profiles in the hydrodynamic focusing device were modeled using finite element method (FEM) simulations to acquire a stationary solution for the diffusive mixing of dendrimers and DNA. Results for these calculations are shown in Figure 2, which includes the profile of concentration of G4 (c_{G4}) as well as the velocity profile within

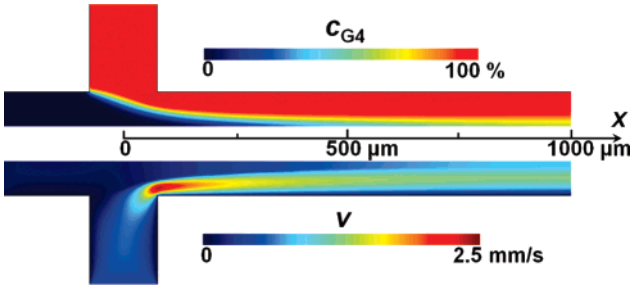

Figure 2. Finite element modeling of conditions within microdevice. Both the concentration of dendrimer c_{G4} (top) and velocity v (bottom) are plotted for one-half of the microchannel device. Scale bar defines $x = 0-1000$ μm.

a channel (the pattern is symmetric; therefore, only half of a device is given). DNA solutions have been assigned a much higher viscosity than the dendrimer solutions ($\eta_{DNA} \approx 10^3 \eta_{G4}$; $\eta_{G4} \approx \eta_{water}$) in the simulations. The calculation of c_{G4} (Figure 2, top) is of particular use since it is directly proportional to the total charge ratio and is used as a defining parameter for the evolution of G4−DNA assemblies. Additionally, the strain rate $\dot{\epsilon} = \partial v/\partial x$ describes the mechanical effects on the material under flow and requires knowledge of the underlying velocity field (Figure 2, bottom).

Small-angle X-ray scattering plays a prominent role as a characterization technique for biomaterials and biological objects in microfluidic systems.[31,32] Spatially resolved microfocused X-ray scattering[33] in hydrodynamic focusing microdevices[34] in particular provides new perspectives in studies of the interaction dynamics of DNA, proteins, and protein assemblies under physiological conditions. Moreover, owing to a concurrent orientation during the assembly process, the characterization of these biomolecular materials, which are difficult to crystallize and normally form liquid−crystalline structures, is significantly improved.[35] Representative X-ray diffraction patterns measured at different distances x from the cross center are shown in Figure 1b. It is important to note that all images reveal oriented diffraction rings, a clear advantage of using flow to assemble G4−DNA complexes. The qualitative differences (i.e., peak width and azimuthal orientation) between these images are readily seen, and the following sections detail what is quantitatively learned from more rigorous analyses of the X-ray patterns.

DNA Mesophase Formation Is Monitored in Real-Time. Small-angle X-ray diffraction data plotted in terms of the reciprocal vector q and obtained via radial integration of the raw image data are given in Figure 3a. The compaction of DNA by G4 dendrimers at different positions x (at $y = 0$) along the reaction channel corresponds to different charge ratios, N/P. Here, N is the total number of positive amine charges of the dendrimers (for full protonation, 62^+ per molecule) and P is the total number of negatively charged phosphate groups of the DNA backbone (2 e^-/base pair). In the first set of experiments, the DNA solution in the main channel was injected with a mean velocity of $v_{DNA} = 100$ μm/s, and the dendrimer solutions were added to the side channel with a mean velocity of $v_{G4} = 4v_{DNA}$. These conditions resulted in a final charge ratio $N/P < 6$ at the furthest measurable point of the device ($x \approx 3$ mm).

Starting at the confluence center of the microchannels ($x = y = 0$), a single peak at $q_0 = 0.2$ Å^{-1} was identified (lowest curve in Figure 3a). Moving the observation position toward larger x, which corresponds to larger N/P ratios, the q_0 peak was shifted toward smaller q values, and a second peak q_1 was concurrently acquired. The ratio $q_1 = \sqrt{2}q_0$ of the two peak positions is consistent with a columnar mesophase with in-plane square symmetry. The lattice constant d of such a unit cell is related to the peak position q_0 using the relation $d = 2\pi/q_0$. An increase in the lattice spacing, d, was obtained at observation points that were further downstream. This can be understood by the incorporation of additional G4 molecules within the G4−DNA assembly.

FEM simulations provide a numerical estimate of the concentration of G4 (c_{G4}) at the channel midpoint for varying x values. The concentration is furthermore transferred into N/P units, assuming that the diffusion of DNA from the center stream outward is much slower than the diffusion of G4 into the center, owing to the former's significantly smaller diffusion coefficient ($D_{DNA} \approx 8 \times 10^{-12}$ m^2/s and $D_{G4} \approx 1.6 \times 10^{-10}$ m^2/s), as was previously shown in the case of collagen.[36] The increase in d (obtained experimentally) is shown in Figure 3c to overlay remarkably well with N/P values (as calculated from FEM, line in Figure 3c) as a function of x, the measurement position in the device. These data are consistent with previously reported bulk X-ray diffraction measurements,[17] citing a two-dimensional columnar lattice of G4−DNA for N/P values $2 \leq N/P < 6$. The precise diffusive mixing of components in flow uniquely allows us to visualize an increase in d over the entire range of columnar mesophases explored here.

Strain Rate $\dot{\epsilon}$ Induces Perpendicular Alignment of Mesophases. The mesoscale alignment of macromolecular assemblies is not easily achieved using standard sample preparation methods; however, alignment in flow is comparatively straightforward using the setup reported here. At the confluence of the microchannels, the main stream was focused, and the fluid elements were accelerated. Owing to this extensional flow, DNA molecules as well as the G4−DNA assemblies experienced an additional hydrodynamic stress, which led to an orientation along the flow direction. Scans of the intensity along the azimuthal angle, χ, on the ring of the q_0 peak at different channel positions x are shown in Figure 3b. Moving outward from $x = 0$ along the reaction channel, all X-ray scans of the dendrimer−DNA assemblies showed a strong orientation preferentially along the flow direction ($\chi \approx -90$ and 90°). The extensional flow led to a favored orientation of the DNA macromolecules parallel to the applied stress (Figure 3e). The degree of orientation can be quantified as the full width at half-maximum of the azimuthal peaks, $\Delta\chi$. Figure 3d clearly shows a minimum value of $\Delta\chi$, corresponding to the highest extent of material orientation, at a position $x = 300$ μm. Remarkably, this behavior is quantitatively predicted in the calculation of strain rate $\dot{\epsilon} = \partial v/\partial \mathbf{x}$ that is provided from the FEM simulations (line, Figure 3d). This indicates that the strain rate can accurately describe the phenomena of supramolecular alignment within microdevices.

The extensive alignment of the G4−DNA assemblies in the region of high strain rate enables the visualization of further details regarding the two-dimensional columnar lattice. That is, we find at $x = 300$ and 400 μm two additional local maxima at $\chi \approx 0$ and 180° (arrows, Figure 3b). This additional weak orientation perpendicular to the flow direction provides interesting insights into the response of a two-dimensional phase of long chain DNA to external stress. The majority of G4−DNA microdomains is oriented parallel to the flow direction. In the region of maximum strain rate, a concomitant orientation of some microdomains perpendicular to the flow direction occurs, most likely due to the structural restrictions imposed by the long DNA strands and square symmetry of the mesophase (schematically represented in Figure 3e).

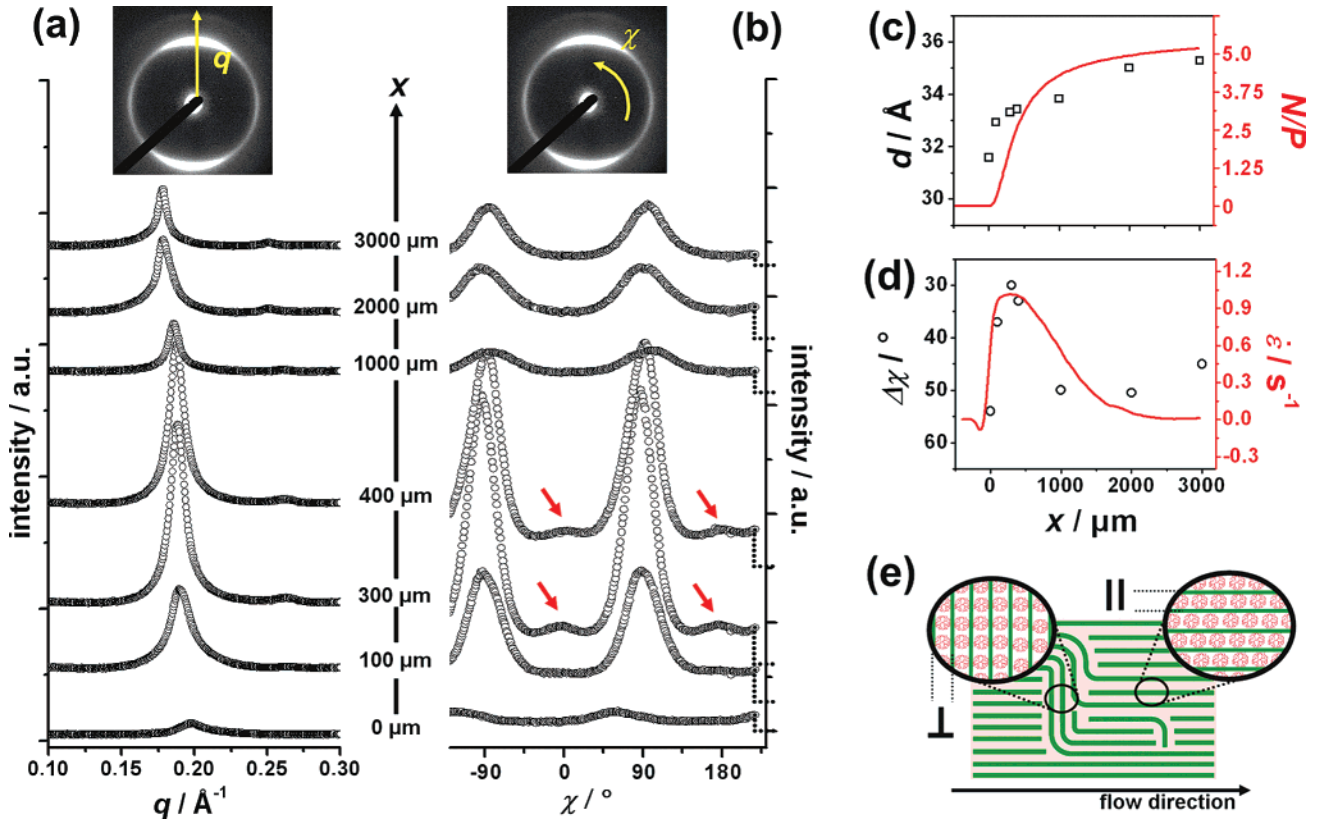

Figure 3. SAXS from varying positions along the microchannel reveals *N*/*P*-dependent lattice spacing and strain-dependent preferential orientation for $v_{DNA} = 100$ μm/s and $v_{G4} = 400$ μm/s. q scans (radial averaging) for a variety of positions x along the microchannel (a) are consistent with a two-dimensional square lattice, having a real space distance d plotted in panel c, which corresponds well to predicted *N*/*P* values (line in c). χ scans (azimuthal integration along peak q_0, note baseline intensity on right-hand side) for the same positions x reveal preferred orientation at $\chi = \pm 90°$ (see schematic in panel e). Degree of preference $\Delta\chi$ (d) is in good agreement with the calculated strain rate (line in panel d). Additional local maxima (arrows in panel b) occur at highest strain rates and correspond to an additional perpendicular ordering (schematic in panel e).

Coexistence of DNA-Enriched and -Depleted Mesophases. The initial stages of DNA compaction leading up to the charge neutral, or isoelectric ($N/P \approx 1.8$),[17] point were conducted by increasing the velocity of the DNA solution and simultaneously reducing the velocity of the dendrimer solutions to $v_{G4} = 3/2v_{DNA}$. Access to this regime is significant because the assembly of G4 mesophases varies as a function of overall charge ratio, conforming to a physical description of charge inversion.[28]

X-ray scans along the *x*- as well as the *y*-direction within the microchannel device are shown in Figure 4. At the center of the confluence of the microchannels (Figure 4b, 0 μm) corresponding to minute dendrimer concentrations, the X-ray pattern appears to be a convolution of multiple peaks with the limiting peak positions $q_{0a} \approx 0.20$ Å^{-1} and $q_{0b} \approx 0.23$ Å^{-1}. Moving to higher $x_{y=0}$ or $y_{x=0}$ values (Figure 4a,b, respectively), corresponding to an increased concentration of dendrimers, the peak at q_{0a} becomes dominant, and the features around q_{0b} disappear. Additionally, the peak position q_{0a} is slightly shifted to smaller q values. Eventually, a second peak $q_1 = \sqrt{2}q_{0a}$ (small arrow, at $x_{y=0} = 1000$ μm and $y_{x=0} = 60$ μm) was recorded, which refers again to a mesoscopic columnar phase with a two-dimensional in-plane square structure. This is surprising given that all measurement points are below the charge neutral point, where there is an excess of negatively charged DNA relative to the amount of G4.

The eventual appearance of q_1 at low dendrimer concentrations—and therefore a surplus of DNA—can be explained by a coexistence of two types of domains: first, positively charged domains with an enrichment of dendrimers and, second, negatively charged domains with a depletion of dendrimers. This is illustrated in Figure 5 from the side (along channel) and front (channel cross-section). The dendrimer-enriched domains show a columnar ordering of the DNA molecules with intercalated

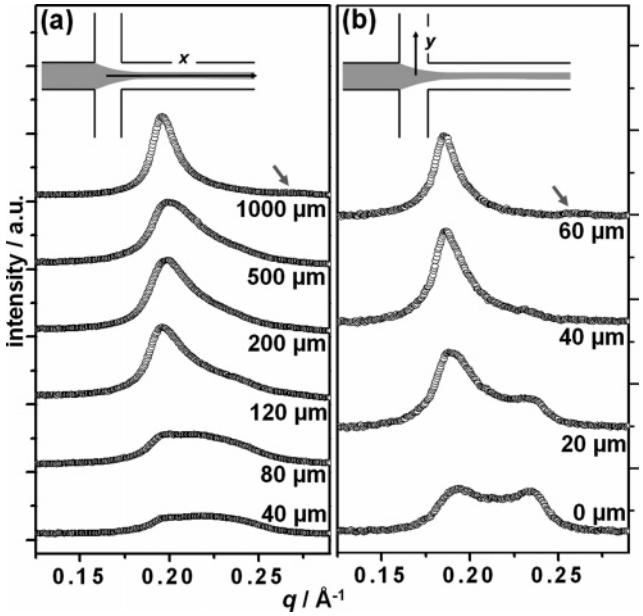

Figure 4. SAXS at $v_{DNA} = 200$ μm/s and $v_{G4} = 300$ μm/s accesses the early stages of DNA compaction by G4. q scans for positions along $x_{y=0}$ (a) and $y_{x=0}$ (b) show the transition from coexistent phases to the square mesophase only, as confirmed by the presence of q_1 at high values of $x_{y=0}$ and $y_{x=0}$ (arrows).

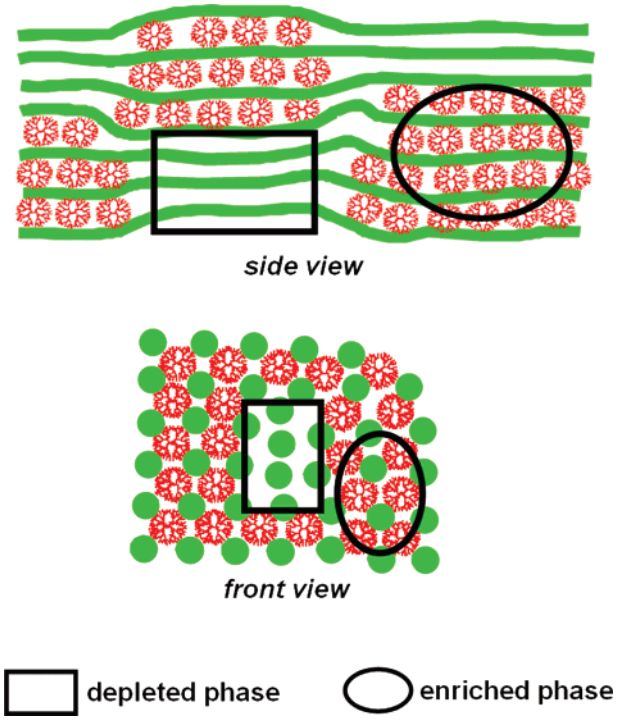

Figure 5. Two coexistent phases in the low dendrimer regime: dendrimer-enriched (circle) and dendrimer-depleted (square). Side view (top) is along the microchannel, and front view (bottom) is a cross-section through the microchannel.

dendrimers, having a spacing $d_{0a} \approx 32$ Å (i.e., the square phase described previously). However, the dendrimer-depleted domains show an ordering of DNA with a spacing that can be calculated from the peak position $q_{0b} \approx 0.23$ Å^{-1} and is dependent on the lattice used to describe the mesophase. We propose that the diffraction peak at position q_{0b} is due to a DNA columnar mesophase with a spacing $d \approx 27$ Å (determined by $d = 2\pi/q$), which indicates very dense DNA packing since it approaches the 25 Å diameter of hydrated DNA molecules. A similar peak at low *N*/*P* values was reported by Evans et al., in which case its striking resemblance to that of hexagonal small cation-induced DNA bundles was noted. In this scenario, the lattice vector $a_H = 4\pi/\sqrt{3}\, q \approx 32$ Å reflects a unit vector on a hexagonal lattice with an interstitial area that is much too small to accommodate a G4 molecule (without requiring a significant molecular deformation).

Regardless of the specific choice of DNA lattice, in either case, we suggest that G4 molecules do not directly bridge the DNA strands. We eliminate dendrimer bridging of DNA strands due to steric constraints: the interstitial positions available to dendrimers in either a square or a hexagonal DNA lattice are too small to accommodate G4 molecules. The dendrimers nevertheless play an important role in the assembly of a one-component DNA mesophase, as is confirmed by experiments performed on DNA solutions without dendrimers that show qualitatively different X-ray patterns.[30] The most reasonable model, by process of elimination, is one including domains rich and poor in G4; this is reminiscent of a scenario reported using DNA and surfactants.[37] The close packing of DNA to length scales $d \approx 27$ Å known to occur in the presence of multivalent salts is considered to be a result of a balance of forces acting to resist (e.g., bending or mixing entropy) or favor (e.g., counterion fluctuations or hydration) condensation.[38] In our case, no additional salts have been explicitly added, but a balance of similar forces is likely at play. The two-phase G4−DNA model is corroborated by a vanishing of the dendrimer-depleted domains ($q_{0a} \leq q \leq q_{0b}$) with a concurrent domination of the square dendrimer−DNA mesophases at increasing $x_{y=0}$ and $y_{x=0}$ values.

Conclusion

We have shown that the potent combination of microfluidics with small-angle X-ray microdiffraction allows for detailed insights into the evolution of DNA compaction in the presence of polypropyleneimine dendrimers. The interactions of dendrimers and DNA are tunable using our microfluidic hydrodynamic focusing device, and X-ray patterns are subsequently acquired at any desired charge ratio *N*/*P* using a microfocused X-ray beam. A two-dimensional columnar phase of dendrimers and DNA has a lattice spacing *d* and degree of orientation $\Delta\chi$ that correspond to the values of *N*/*P* and the strain rate, respectively, both of which are calculated using FEM.

A major advantage of the data shown here is the acquisition of multiple *N*/*P* data points on a single device while using extremely small amounts of material without concern (due to the continuous flow of materials) for X-ray radiation damage. An added benefit of the experimental setup is the resulting alignment of materials within the device. Aligned samples provide additional information regarding the liquid crystalline order of the material and have improved diffraction statistics. Subsequently, detector exposure times were only 30 s per image, and all images exhibited an orientation of the materials along the direction of flow. The G4−DNA system displays a striking response to the extensional flow that is created within the microchannel. Namely, the mesophases align transverse to the flow direction at a point in the microdevice where the strain rate is highest, an interpretation of which is illustrated in Figure 3e.

We are also able to access, for the first time in a controlled manner, very low *N*/*P* ratios where a coexistence of DNA−DNA and dendrimer−DNA interactions appears to occur. Generally, DNA is considered to condense in biological systems via multivalent salts or proteins.[1,39,40] Our results indicate that in an undercharged (low *N*/*P*) regime, it is also possible that DNA condensation occurs without direct contact to such materials. This phase may also exist in biological cells, which are dense and contain a variety of surrounding protein aggregates. In addition, the stages of DNA packing and ejection in bacteriophage are a subject of considerable biophysical interest and involve dense packing of DNA suggestive of the assembly found here for low *N*/*P* values.[41]

Using more elaborate microfluidic designs, the results reported here can be extended to study the complexity of hierarchical self-organization and, moreover, to generate in vitro models that mimic the biological process of DNA aggregation. This can be achieved with the incorporation of additional microfluidic inlets, which would allow the introduction of further compacting agents such as the linker histone H1, as well as through the integration of more sophisticated channel design elements that impose well-predicted mechanical forces on the mesophases. These strategies are facilitated by a new generation of elastomeric microflow foils, which allow rapid design prototyping.[15] Furthermore, the creation and conformational control of new nanostructured materials with biological activity is enabled by fine-tuning the physical and chemical parameters (e.g., condensation agents and solvent) for a variety of macromolecular systems including, but certainly not limited to, protein scaffolds, enzymatic reactions, and polymeric materials for drug release.

Acknowledgment. We gratefully acknowledge fruitful discussions with Stephan Herminghaus, Dagmar Steinhauser, Anatoly Snigirev, and Oleg Konovalov and thank Udo Krafft for excellent technical assistance. We acknowledge the ESRF for provision of synchrotron radiation facilities at beamline ID10b. H.M.E. acknowledges a fellowship from the Alexander von Humboldt Foundation. This work was supported by the DFG within the Emmy-Noether-Program (PF 375/2).

References and Notes

(1) Martinez, A.; Kolter, R. *J. Bacteriol.* **1997**, *179*, 5188−5194.
(2) Wolf, S. G.; Frenkiel, D.; Arad, T.; Finkel, S. E.; Kolter, R.; Minsky, A. *Nature* **1999**, *400*, 83−85.
(3) Minsky, A.; Shimoni, E.; Frenkiel-Krispin, D. *Nat. Rev. Mol. Cell Biol.* **2002**, *3*, 50−60.
(4) Gelbart, W. M.; Bruinsma, R. F.; Pincus, P. A.; Parsegian, V. A. *Phys. Today* **2000**, *53*, 38−44.
(5) Durand, D.; Doucet, J.; Livolant, F. *J. Phys. II* **1992**, *2*, 1769−1783.
(6) Rädler, J. O.; Koltover, I.; Salditt, T.; Safinya, C. R. *Science* **1997**, *275*, 810−814.
(7) Topp, A.; Bauer, B. J.; Prosa, T. J.; Scherrenberg, R.; Amis, E. J. *Macromolecules* **1999**, *32*, 8923−8931.
(8) Boas, U.; Heegaard, P. M. H. *Chem. Soc. Rev.* **2004**, *33*, 43−63.
(9) Kukowska-Latallo, J. F.; Bielinska, A. U.; Johnson, J.; Spindler, R.; Tomalia, D. A.; Baker, J. R. *Proc. Natl. Acad. Sci. U.S.A.* **1996**, *93*, 4897−4902.
(10) Pack, D. W.; Hoffman, A. S.; Pun, S.; Stayton, P. S. *Nat. Rev. Drug Discovery* **2005**, *4*, 581−593.
(11) Dufes, C.; Uchegbu, I. F.; Schatzlein, A. G. *Adv. Drug Delivery Rev.* **2005**, *57*, 2177−2202.
(12) Bosman, A. W.; Janssen, H. M.; Meijer, E. W. *Chem. Rev.* **1999**, *99*, 1665−1688.
(13) Scherrenberg, R.; Coussens, B.; van Vliet, P.; Edouard, G.; Brackman, J.; de Brabander, E.; Mortensen, K. *Macromolecules* **1998**, *31*, 456−461.
(14) Kabanov, V. A.; Sergeyev, V. G.; Pyshkina, O. A.; Zinchenko, A. A.; Zezin, A. B.; Joosten, J. G. H.; Brackman, J.; Yoshikawa, K. *Macromolecules* **2000**, *33*, 9587−9593.
(15) Dootz, R.; Evans, H. M.; Köster, S.; Pfohl, T. *Small* **2007**, *3*, 96−100.
(16) Burghardt, W. R.; Brown, E. F.; Auad, M. L.; Kornfield, J. A. *Rheol. Acta* **2005**, *44*, 446−456.
(17) Evans, H. M.; Ahmad, A.; Ewert, K.; Pfohl, T.; Martin-Herranz, A.; Bruinsma, R. F.; Safinya, C. R. *Phys. Rev. Lett.* **2003**, *91*, 75501-1−75501-4.
(18) Liu, Y. C.; Chen, H. L.; Su, C. J.; Lin, H. K.; Liu, W. L.; Jeng, U. S. *Macromolecules* **2005**, *38*, 9434−9440.
(19) Beebe, D. J.; Mensing, G. A.; Walker, G. M. *Annu. Rev. Biomed. Eng.* **2002**, *4*, 261−286.
(20) Hansen, C.; Quake, S. R. *Curr. Opin. Struct. Biol.* **2003**, *13*, 538−544.
(21) Song, H.; Tice, J. D.; Ismagilov, R. F. *Angew. Chem., Int. Ed.* **2003**, *42*, 768−772.
(22) Whitesides, G. M. *Nat. Biotechnol.* **2003**, *21*, 1161−1165.
(23) Zheng, B.; Tice, J. D.; Roach, L. S.; Ismagilov, R. F. *Angew. Chem., Int. Ed.* **2004**, *43*, 2508−2511.
(24) Pfohl, T.; Mugele, F.; Seemann, R.; Herminghaus, S. *Chem. Phys. Chem.* **2003**, *4*, 1291−1298.
(25) Köster, S.; Steinhauser, D.; Pfohl, T. *J. Phys.: Condens. Matter* **2005**, *17*, 4091−4104.
(26) Bloomfield, V. A. *Biopolymers* **1997**, *44*, 269−282.
(27) Raspaud, E.; de la Cruz, M. O.; Sikorav, J. L.; Livolant, F. *Biophys. J.* **1998**, *74*, 381−393.
(28) Grosberg, A. Y.; Nguyen, T. T.; Shklovskii, B. I. *Rev. Mod. Phys.* **2002**, *74*, 329−345.
(29) Snigirev, A.; Kohn, V.; Snigireva, I.; Lengeler, B. *Nature* **1996**, *384*, 49−51.
(30) Dootz, R.; Otten, A.; Köster, S.; Struth, B.; Pfohl, T. *J. Phys.: Condens. Matter* **2006**, *18*, 639−652.
(31) Pollack, L.; Tate, M. W.; Darnton, N. C.; Knight, J. B.; Gruner, S. M.; Eaton, W. A.; Austin, R. H. *Proc. Natl. Acad. Sci. U.S.A.* **1999**, *96*, 10115−10117.
(32) Pollack, L.; Tate, M. W.; Finnefrock, A. C.; Kalidas, C.; Trotter, S.; Darnton, N. C.; Lurio, L.; Austin, R. H.; Batt, C. A.; Gruner, S. M.; Mochrie, S. G. J. *Phys. Rev. Lett.* **2001**, *86*, 4962−4965.
(33) Otten, A.; Köster, S.; Struth, B.; Snigirev, A.; Pfohl, T. *J. Synchrotron Radiat.* **2005**, *12*, 745−750.
(34) Knight, J. B.; Vishwanath, A.; Brody, J. P.; Austin, R. H. *Phys. Rev. Lett.* **1998**, *80*, 3863−3866.
(35) Bouxsein, N. F.; Hirst, L. S.; Li, Y. L.; Safinya, C. R.; Abu Samah, Z.; MacDonald, N. C.; Pynn, R. *Appl. Phys. Lett.* **2004**, *85*, 5775−5777.
(36) Köster, S.; Leach, J. B.; Struth, B.; Pfohl, T.; Wong, J. Y. *Langmuir* **2007**, *23*, 357−359.
(37) Ghirlando, R.; Wachtel, E. J.; Arad, T.; Minsky, A. *Biochemistry* **1992**, *31*, 7110−7119.
(38) Bloomfield, V. A. *Biopolymers* **1991**, *31*, 1471−1481.
(39) Wolffe, A. *Chromatin Structure and Function*; Academic Press: San Diego, 1998.
(40) Ames, B. N.; Dubin, D. T. *J. Biol. Chem.* **1960**, *235*, 769−775.
(41) Purohit, P. K.; Inamdar, M. M.; Grayson, P. D.; Squires, T. M.; Kondev, J.; Phillips, R. *Biophys. J.* **2005**, *88*, 851−866.

BM070317S